Nonlinear mode interactions and period-tripling flutter in transonic flow

O.O. Bendiksen*

Mechanical and Aerospace Engineering Department, University of California, Los Angeles, CA 90095-1597, USA

Abstract

Near Mach one, the aerodynamic nonlinearities become of first order and can no longer be neglected in flutter calculations. Because the superposition principle also breaks down, aeroelastic modes cannot simply be added in a linear manner, as done in the $U–g$ and $p–k$ methods of flutter analysis. This paper discusses two nonlinear phenomena of relevance in transonic flutter analysis and testing: (i) multibranch flutter caused by nonlinear mode interactions, and (ii) the sudden emergence of a fundamentally different nonlinear flutter mode via a period-tripling bifurcation. In the first case, the superposition principle is not valid and flutter may not necessarily occur when the first aeroelastic eigenvalue crosses into the right half-plane. In the second case, the nonlinearities open up a new route to flutter, whereby the reduced frequency of the critical aeroelastic mode is lowered into the unstable range through the period-tripling bifurcation, and an entirely new flutter mode is born. Neither behavior can be understood within the theory of classical linear aeroelasticity.
© 2004 Published by Elsevier Ltd.

1. Introduction

Linear flutter stability concepts have been very successful in "explaining" the observed flutter behavior of aircraft wings at subsonic Mach numbers, below the transonic region; see, for example, Theodorsen and Garrick (1940), Garrick (1946), and Bisplinghoff and Ashley (1962). Although nonlinear time-marching flutter calculations in the transonic region have by now become routine, the interpretation of the calculated stability behaviors continues to rely on ideas from classical linear aeroelasticity. For example, it is generally assumed that flutter occurs at the lowest speed at which any one of the aeroelastic eigenvalues crosses into the unstable (right) half-plane. This principle is the cornerstone of the classical linear $U–g$ and $p–k$ methods of flutter analysis, where individual aeroelastic modes are traced vs. airspeed or Mach number to determine where flutter first occurs.

The objective of this paper is to show that there appear to be exceptions to this rule, where the superposition principle for aeroelastic modes breaks down and flutter does not occur when the first aeroelastic eigenvalue crosses into the right half-plane. This in turn implies that there exist flutter instabilities that cannot be predicted by formulating and solving a classical linear aeroelastic eigenvalue problem, and that the stability concepts from classical aeroelasticity may need to be modified.

Recent nonlinear Euler-based calculations (Bendiksen, 2002) reveal that near the transonic dip, the critical aeroelastic mode is a *multibranch mode*, because a single-degree-of-freedom (SDOF) torsional flutter instability exists at the bottom

---

*Fax: + 1-310-206-4830.

  E-mail address: oddvar@seas.ucla.edu (O.O. Bendiksen).

Nomenclature

a	speed of sound; also location of elastic axis
A	wing aspect ratio
c	$2b =$ airfoil or wing chord
C_L, C_M	lift and moment coefficients
C_p	pressure coefficient
E_{tot}	$T + U =$ total energy
g	structural (hysteresis) damping
h	plunge (bending) displacement at elastic axis (EA), positive down
k	$\omega b/U_\infty =$ reduced frequency
l	wing semispan
m	mass per unit span
M	Mach number
p	pressure
q	$\frac{1}{2}\rho_\infty U_\infty^2 =$ dynamic pressure
q_i	generalized coordinates
t	time
T	kinetic energy; also absolute temperature
$\bar{U}$	$U_\infty/b\omega_\alpha =$ reduced velocity
U	strain energy
U_∞	freestream velocity at upstream infinity
α	local angle of attack
δ	wing thickness ratio, $t_{\max}/c$
θ	wing elastic twist
μ	$m/\pi\rho b^2 =$ mass ratio
ρ	air density
τ	nondimensional time $= \omega_\alpha t$
χ	transonic similarity parameter (aerodynamic)
Ψ	transonic similarity parameter for flutter
ω	circular frequency, rad/s
ω_h	uncoupled bending mode frequency in vacuum
ω_α	uncoupled torsion mode frequency in vacuum

Superscripts and subscripts

F	flutter
$(\tilde{\ })$	similarity function
∞	conditions at upstream infinity

of the transonic dip. At intermediate mass ratios the SDOF flutter can usually only be observed indirectly, through its interactions with the primary bending–torsion mode, even in cases where the torsional root is unstable. In this case the classical principle of critical (minimum) flutter speed appears to be violated, and stability cannot be determined by considering the stability of the individual linearized aeroelastic modes. The present paper presents a more detailed exploration of this phenomenon and the apparent breakdown of classical aeroelastic stability concepts.

At very low mass ratios, linear aerodynamic theories predict that flutter is impossible because the reduced frequency becomes too high; see, for example, the results and discussion in Ashley's study (Ashley, 1980) of subtransonic flutter (e.g. Fig. 10 of that reference). In the transonic region, however, we show that the flutter speed does not approach infinity at very low mass ratios (below about 5), as predicted by subsonic linear aerodynamics. Instead, the aerodynamic nonlinearities open up a new route to flutter, by lowering the reduced frequency of the critical aeroelastic mode into the unstable range through a *period-tripling* bifurcation. This flutter occurs at a frequency *outside* the first bending–first torsion frequency interval, and cannot be understood within a linear flutter analysis framework.

2. Theoretical considerations

2.1. Nonlinear aeroelastic models

If linear aeroelastic stability concepts are inadequate in transonic flow, what are the alternatives? At first glance it would appear that bifurcation theory provides the natural tools and ideas for analyzing and understanding nonlinear aeroelastic instabilities. Indeed, there are nonlinear fluid–structure interaction and stability problems where the formal theory can be of great help in classifying and interpreting the possible instabilities. But these are generally problems where the essential dynamics can be captured using relatively simple models based on ordinary differential equations (ODEs). It is then often possible to obtain a highly reduced model, of the generic form

$$\dot{x} = F(x, \lambda), \tag{1}$$

where only the essential degrees of freedom are retained. Here x is a suitable nondimensional state vector for the structural system, in terms of the generalized coordinates q_i and velocities $\dot{q}_i$, and λ is a set of nondimensional flutter parameters.

Notwithstanding the immense literature on Eq. (1) [see, for example, Guckenheimer and Holmes (1983)], the model is very restrictive from an aeroelastic perspective, since it assumes that the unsteady aerodynamic forces are expressible as point functions of the structural state of the system. This basically implies a quasisteady aerodynamic theory, or a supersonic piston theory, or certain other very special cases, such as internal flows in pipes, for example. Thus, although Eq. (1) may be suitable for studying quasisteady flutter and divergence problems of wings, panel flutter at high supersonic Mach numbers, and flutter and divergence of slender pipes carrying a fluid, it does not provide the correct framework for modelling the unsteady aerodynamics of wings and lifting surfaces.

In the general aeroelastic problem associated with aircraft wings, the function F must be replaced by a *functional* that depends not only on the present state of the system but also on the entire time history of the motion, x_t:

$$x_t(s) = x(t + s), \quad -\infty < s \leqslant 0, \tag{2}$$

$$\dot{x} = \aleph(x_t, \lambda), \tag{3}$$

where the nonlinear functional $\aleph$ has "memory"; it remembers past motions through the effect of the shed vorticity from the trailing edge and from the entropy production at the shocks. This leads to differential–functional equations with infinite time delays, which are much more difficult to treat, but which provide a much richer and infinite-dimensional eigenspace of aeroelastic solutions (Hale and Verduyn Lunel, 1993).

Anderson (1993,1995) has argued that for certain aeroelastic system possessing an appropriate "fading memory property", the qualitative aeroelastic response can be deduced from a set of finite-dimensional ordinary differential equations of the form of Eq. (1). From our analysis, this would seem equivalent to assuming the existence of an "equivalent" quasisteady aerodynamic operator. Whether this assumption can lead to a satisfactory approximation in the transonic range is still an open question, because the shock motion amplitudes and phase angles are not well behaved in the quasisteady limit

$$k = \frac{\omega b}{U_\infty} \to 0^+. \tag{4}$$

In transonic flutter problems, we believe that the difference between Eqs. (1) and (3) is of importance. For example, it is the memory effect in Eq. (3) that is responsible for certain dynamic hysteresis phenomena observed in numerical simulations and in some of the secondary flutter bifurcations.

Despite its limitations, Eq. (1) provides a starting point for our analysis, in the same way that a quasisteady flutter analysis can reveal much of the stability behavior of low-frequency, low Mach number flutter. By performing a Taylor expansion of F about the zero equilibrium position, Eq. (1) can be put in the form

$$\dot{x} = A(\lambda)x + f(x, \lambda), \tag{5}$$

where A is the Jacobian matrix at $x = 0$ and f is the nonlinear part of F. The linearized system is obtained from Eq. (5) by neglecting f. The eigenvalues of the linear matrix A depend on the bifurcation parameters $\lambda = \{\lambda_1, \lambda_2, ..., \lambda_p\}^{\mathrm{T}}$, which in turn determines the bifurcation. For a typical section model in inviscid flow, there are three primary parameters: Mach number M, reduced velocity $\bar{U}$, and mass ratio μ. Additionally, there are four typical sections parameters: a, x_α, r_α and ω_h/ω_α. In most flutter calculations, the section parameters are kept fixed and the three primary variables M, $\bar{U}$, and μ are varied.

For hyperbolic equilibrium points, where none of the eigenvalues of A has a zero real part, the stability of the solutions near $x = 0$ is determined by the linearized equations (Guckenheimer and Holmes, 1983). The interesting cases in aeroelastic stability problems involve nonhyperbolic equilibrium points, where one or more of the eigenvalues of A

has a zero real part and the stability of the bifurcated solutions cannot be determined without considering the nonlinear terms in the equations.

The Hopf bifurcation is often considered as a prototype bifurcation for modelling flutter. In this bifurcation, a pair of complex conjugate eigenvalues of the matrix A crosses the imaginary axis with nonzero speed, and the stable zero equilibrium point bifurcates into a limit cycle. Numerical simulations of aeroelastic systems in the time domain involve another discretization of the equations, to obtain a space-and-time-discretized aeroelastic model of the form of a nonlinear map

$$x^{n+1} = G(x^n, \lambda), \tag{6}$$

where the vector function G provides a numerical recipe for advancing the solution from the nth to the $(n+1)$th time step; $t^n \rightarrow t^{n+1} = t^n + \Delta t$. For explicit time integrations schemes, such as the multistage Runge–Kutta scheme used in this paper, expressions for the components of G can be written down. In the simultaneous integration of the fluid and structural equations, the state vector x in the map includes the fluid degrees of freedom, and is therefore very large. In the classical approach, the structural degrees of freedom are favored and the fluid degrees of freedom are condensed out during the time-marching procedure.

2.2. Transonic similarity laws

The transonic flutter boundaries are sensitive to wing thickness and angle of attack, and this dependence can be deduced from the transonic similarity principles and scaling laws presented by Bendiksen (1999). The idea is to consider a family of "similar" wings of the same airfoil shape, Fig. 1, by scaling the wing profile

$$F_{u,l}(x, y) = \delta f_{u,l}(x, y), \tag{7}$$

where δ is a nondimensional thickness (scaling) parameter, $f_{u,l}(x, y)$ represents the rigid (jig) wing shape, and subscripts u and l denote upper and lower surfaces, respectively. For small angles of attack and small elastic deformations, the equation for the wing surface is given by

$$B(x, y, z, t) = z - \delta \left\{ f_{u,l}(x, y) + \frac{[w(y, t) - x\alpha(y, t)]}{\delta} \right\} = 0. \tag{8}$$

For unsteady transonic flow, the similarity parameters are

$$\chi = \frac{1 - M_\infty^2}{[(\gamma + 1)M_\infty^2 \delta]^{2/3}}, \quad \tilde{A} = [(\gamma + 1)M_\infty^2 \delta]^{1/3} A,$$

$$\tilde{\alpha} = \alpha/\delta, \quad \tilde{w} = w/\delta, \quad \tilde{t} = \frac{\delta^{2/3} t}{[(\gamma + 1)M_\infty^2]^{1/3}}, \tag{9}$$

where γ is the ratio of specific heats and A is the aspect ratio of the wing. The similarity rules for the steady aerodynamic lift and moment coefficients can then be stated in the form

$$C_L = \frac{\delta^{2/3}}{[(\gamma + 1)M_\infty^2]^{1/3}} \tilde{C}_L(\chi, \tilde{A}, \tilde{\alpha}), \tag{10}$$
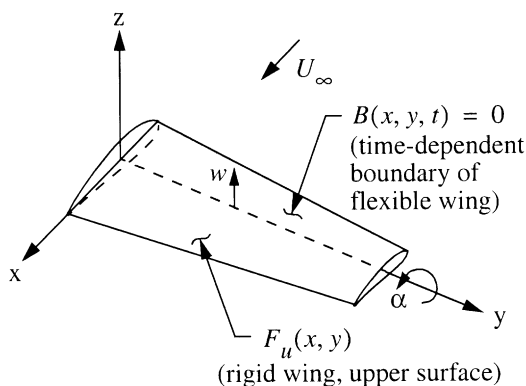

Fig. 1. Wing coordinate system and surface definition.

$$C_M = \frac{\delta^{2/3}}{[(\gamma+1)M_\infty^2]^{1/3}} \tilde{C}_M(\chi, \tilde{A}, \tilde{\alpha}), \tag{11}$$

where "similarity functions" $\tilde{C}_L$ and $\tilde{C}_M$ are functions of the three similarity parameters χ, $\tilde{A}$, and $\tilde{\alpha}$. Similar flows have the same pressure distributions, lift, moment, drag, etc., after they have been rescaled as specified by the similarity rules.

For aeroelastic similarity, the transonic flutter similarity parameter

$$\psi = \frac{\bar{U}^2}{\pi\mu[(\gamma+1)M_\infty^2\delta]^{1/3}} = \frac{\frac{1}{2}\rho_\infty U_\infty^2}{\frac{1}{2}m\omega_\alpha^2} \frac{1}{[(\gamma+1)M_\infty^2\delta]^{1/3}} \equiv \frac{\hat{q}}{[(\gamma+1)M_\infty^2\delta]^{1/3}} \tag{12}$$

must also be kept fixed, where $\hat{q}$ is a nondimensional dynamic pressure

$$\hat{q} = \frac{\frac{1}{2}\rho_\infty U_\infty^2}{\frac{1}{2}m\omega_\alpha^2} = \frac{\bar{U}^2}{\pi\mu} = \frac{1}{\pi}\left(\frac{U}{b\omega_\alpha\sqrt{\mu}}\right)^2. \tag{13}$$

To keep the reduced frequency $k = \omega b/U_\infty$ fixed, the reduced airspeed $\bar{U} = U_\infty/b\omega_\alpha$ must be held constant.

In the inviscid case, there are three primary similarity parameters: χ, Ψ, and $\bar{U}$. In viscous flows, the Reynolds number provides a fourth similarity parameter. In addition, we must include the dynamical similarity parameters for the wing itself, which in the simplest case of a typical section model consist of the four parameters a, x_α, r_α, and ω_h/ω_α. In comparing the aeroelastic response, consideration must also be given to the amplitude scaling, as reflected through the similarity parameters $\tilde{\alpha}$ and $\tilde{w}$.

2.3. Transonic flutter boundary

In the study by Bendiksen (2002), it was shown that is not possible to get a complete picture of the transonic flutter behavior of a wing from classical two-parameter plots of the linear flutter speed, or dynamic pressure, vs. Mach number. For a given aeroelastic model, the flutter boundary may be plotted as a surface in a three-dimensional parameter space, Fig. 2, where the axes represent the three primary similarity parameters. Using the transonic similarity parameters χ, Ψ, and $\bar{U}$ would provide the most general plots, allowing for changes in airfoil thickness and test medium, but for a given model it is permissible to plot the surface using the classical flutter variables M_∞, μ, and $\bar{U}$, as done in Fig. 2.
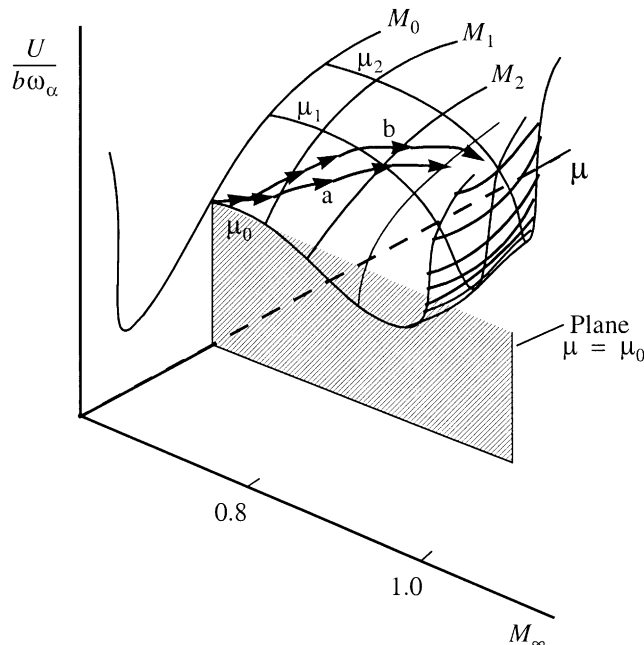

Fig. 2. Flutter boundary as a surface in a 3-D space of classical similarity parameters, with all other model parameters fixed. The observed flutter boundaries in wind tunnel tests are represented by curves or paths (a,b, …) on this surface, and may differ from test to test if the temperature changes.

From Fig. 2 we see that a 2-D plot of $\bar{U}_F$ vs. M_∞ (for a fixed mass ratio μ_0) represents the projection of the actual 3-D flutter curve "a" or "b" on the plane $\mu = \mu_0$, parallel to the $(\bar{U}_F, M_\infty)$ coordinate plane. There is a corresponding projection, for each Mach number, of the 3-D flutter curve onto a plane parallel to the $(\bar{U}, \mu)$ coordinate plane and passing though the Mach number being considered. Because the actual path traced out on the flutter surface depends not only on the properties of the aeroelastic model, but also on the properties of the wind tunnel and the test procedure used, the two-parameter projections on the similarity planes are not unique for a given aeroelastic model. Furthermore, the nature (location, sharpness, etc.) of the transonic dip depends on the path traced out on the flutter surface, and on the angle at which the "transonic valley" is entered. This can lead to confusion when attempting to interpret transonic flutter data based on two-parameter plots.

In theoretical or computational flutter calculations, the mass ratio is usually kept fixed and the flutter boundary is plotted as $\bar{U}$ or $\bar{U}/\sqrt{\mu}$ vs. M_∞. In wind tunnel flutter tests, on the other hand, both the Mach number M_∞ and the density typically change from point to point, with μ often varying over an order of magnitude (or more) in a given test. The airspeed is fixed by the relation

$$U_\infty = M_\infty a_0 \sqrt{\theta}, \tag{14}$$

where a_0 is the speed of sound at SLSD conditions and $\theta = T/T_0$ is the absolute temperature ratio. If the temperature is constant, then U and $\bar{U}$ will be directly proportional to the freestream Mach number M_∞. But if the temperature is not constant during the test (or between different testing days), the slope of U vs. M_∞ will change, which will alter the reduced frequency and mass ratio at which flutter is encountered, and hence also the flutter boundary $\bar{U}_F$ or q_F vs. M_∞. Because the sensitivity to temperature depends on the local slope, $\partial \bar{U}_F/\partial \mu$, different aeroelastic models will generally show different sensitivity to changes in temperature. Note that the 3-D flutter surface is unaffected by temperature changes.

It is therefore important to distinguish between flutter boundaries at constant mass ratio (altitude), and boundaries obtained in a variable-density wind tunnel. As is shown in Fig. 3, the two cases may yield completely different boundaries in the transonic region, even for the same aeroelastic model. For a detailed discussion of this important point, see Bendiksen (2002).

In this paper two different typical section aeroelastic models are used in the time-marching calculations, with parameters as shown in Table 1. The first is an NACA 0006 typical section model studied by Lazarus et al. (1991) and also by Bendiksen (1997a). The second model is an NACA 0012 airfoil with typical section parameters identical to the NACA 0012 Benchmark Model tested at the NASA Langley Research Center (Rivera et al., 1992). The time-marching flutter calculations were made using the direct Eulerian–Lagrangian scheme (Bendiksen, 1991), with a modified typical section of unit width modelled with eight plate finite elements. A 192×32 C-mesh was used in the fluid domain. For the NACA 0012 model, six FEMS and a 144×24 mesh were used.

3. Multibranch flutter

3.1. Which flutter mode?

Transonic flutter and the transonic dip cannot be fully understood in terms of classical bending–torsion coalescence flutter, for the simple reason that this is not the correct instability mechanism in the transonic region. In the classical linear U–g or p–k methods of flutter analysis, where individual aeroelastic modes are traced vs. airspeed or Mach number, an undue emphasis is placed on the mode frequencies and their tendencies to (or not to) coalesce. The corresponding changes in the flutter mode are often ignored; in fact, the mode amplitude ratios may not even be calculated and are seldom if ever plotter in a standard flutter analysis. This is unfortunate, because changes in the flutter mode (amplitude ratio(s) and phase(s)) are often much better physical indicators of the true nature of the instability mechanism than are the corresponding changes in the mode frequencies, especially at transonic Mach numbers.

Near and inside the transonic dip, the flutter mode undergoes a rapid change over a relatively narrow Mach number interval. Recent calculations have revealed that, for sufficiently high mass ratios, *multibranch flutter* occurs. That is, two (or more) aeroelastic modes are "active" and competing for attention in the aeroelastic response. From a linear stability point of view, the aeroelastic response would be expected to be a linear superposition of all aeroelastic modes,

$$\sum_i c_i \{q\}_i e^{p_i t}, \tag{15}$$

where $\{q\}_i$ is the (complex) aeroelastic eigenvector corresponding to the eigenvalue p_i and the c_i are constants that depend on the initial conditions. In subsonic flutter, the damping levels of the aeroelastic modes differ sufficiently to
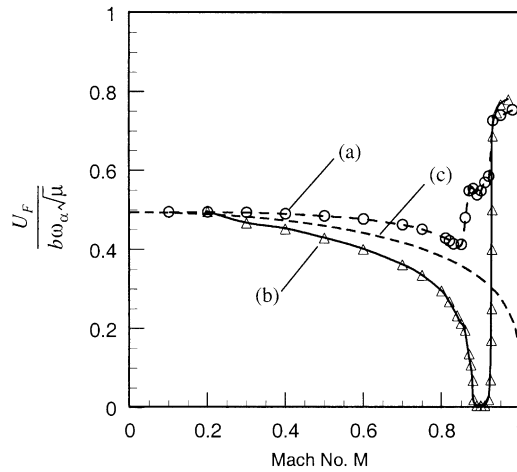
Fig. 3. (a) Flutter boundary for NACA 0006 model, corresponding to fixed mass ratio $\mu = 20$; (b) corresponding boundary if $U_\infty = a_\infty \mathrm{M}_\infty$ and μ is decreased until flutter occurs; (c) Theodorsen–Garrick rule for subsonic flutter. ((a and b) from nonlinear Euler-based calculations).

Table 1
Aeroelastic models

Model	a	x_α	r_α^2	ω_h/ω_α	μ[a]
NACA 0006	-0.20	0.20	0.25	0.20	20
NACA 0012	0.0	0.0	0.25[b]	0.6462	75

[a] For cases where mass ratio is kept constant.
[b] Except as noted (Benchmark model nominal $r_\alpha^2 = 1.024$).
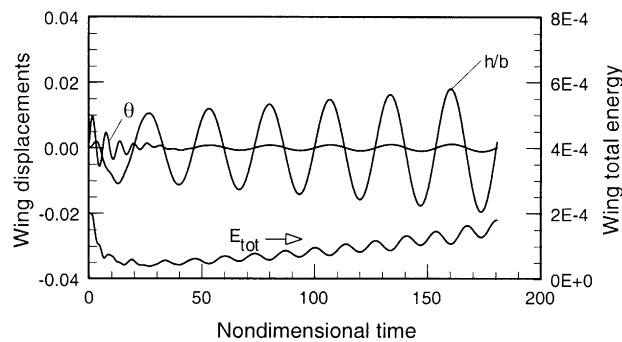
Fig. 4. Bending–torsion flutter mode of NACA 0006 model at Mach 0.86, with $\mu = 1800$; $\bar{U} = 9.525$; $\dot{\alpha}(0) = 0.02$.

ensure that a well-defined flutter mode quickly emerges. Because the aeroelastic branches diverge exponentially, only the least stable mode is generally observable in time-marching calculations and in wind tunnel tests. This is illustrated in Fig. 4, which shows the flutter mode for the NACA 0006 model at Mach 0.86. Note that although the initial conditions only excite the torsion mode, the bending-branch flutter mode quickly emerges.

But in the transonic case, both the first bending and first torsion branches can be brought to flutter at Mach numbers near the transonic dip, by adjusting the mass ratio. Fig. 5 shows this type of flutter for the NACA 0006 model. An essentially SDOF torsional flutter is about to emerge, but must compete for attention with the bending branch. Part (a) shows that the bending branch is on a limit cycle and the torsion branch is lightly damped, when the mass ratio is 1600 and $\bar{U} = 5.9$. Increasing the mass ratio to 5000 and $\bar{U}$ to 8.5 brings the torsion branch to a limit cycle, while the bending
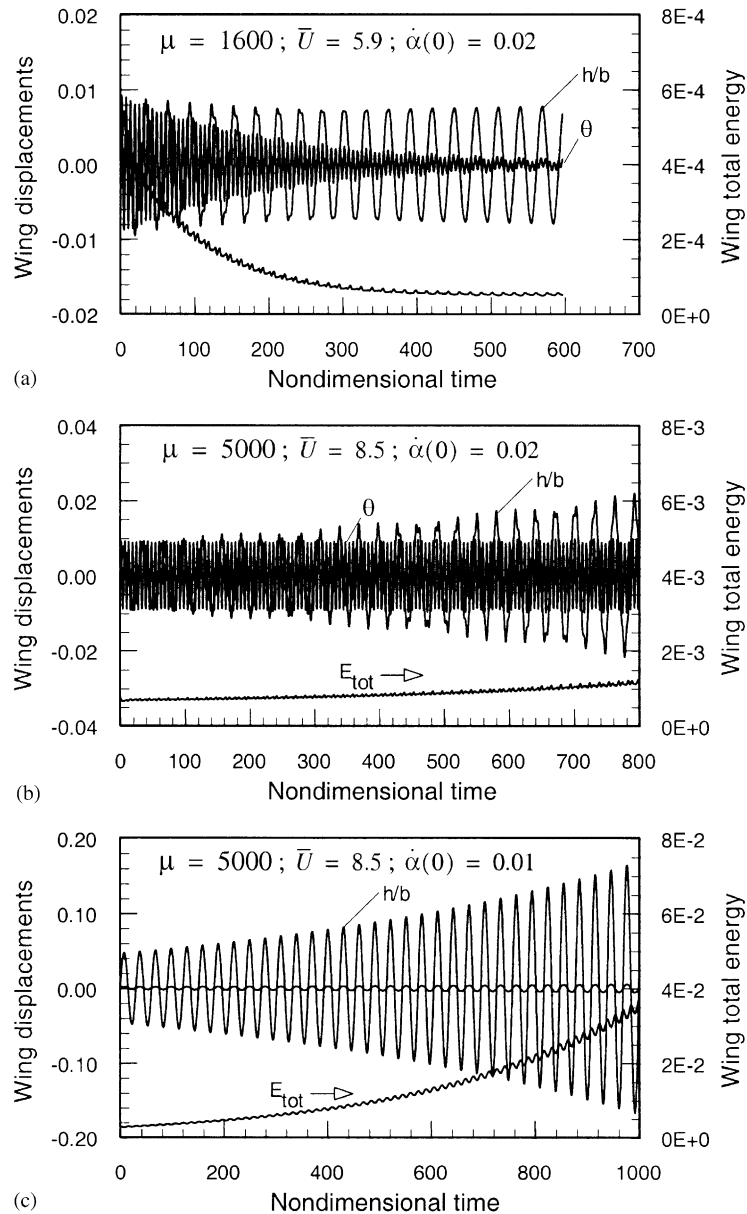
Fig. 5. Multibranch flutter of NACA 0006 model at Mach 0.882. Note sensitivity to initial conditions.

branch now displays divergent flutter. But if the initial conditions are changed slightly, the torsion branch is suppressed and never emerges, Fig. 5(c), even though the mode is (linearly) unstable. The frequencies of the first bending and first torsion flutter mode branches remain far apart, both before and after flutter has occurred for either branch. Thus, the flutter mechanism cannot be attributed to classical bending–torsion coalescence flutter. In fact, there is little or no evidence that changes in the mode frequencies play a significant role in bringing about the flutter in either of the mode branches. But it would be incorrect to assume that the flutter is not of the coupled bending–torsion type, at least as far as the bending branch is concerned. Calculations of the energy transfer from the air to the wing indicate that a pure bending oscillation is stable in subsonic and transonic flows, for all reduced frequencies (Bendiksen, 2001). This is in agreement with the observations of Ashley (1980) that some pitching motion must occur even in those "SDOF" bending flutter cases reported in the literature.

Another case of multibranch flutter is shown in Fig. 6. Here, both the bending and torsion branches are unstable from the start. At $\tau \cong 500$, after about 80 oscillation periods, the torsion branch appears to bifurcate to a more strongly

unstable torsional mode, which subsequently "quenches" the bending branch. This quenching phenomenon has been observed in several other instances of multibranch flutter, including cases where the flutter branches interact with the weak divergence branch (Bendiksen, 1997b). It is a nonlinear phenomenon, which violates the superposition principle of linear aeroelastic modes, and thus also the associated stability concepts of linear aeroelasticity.

3.2. SDOF torsional flutter

Although SDOF bending flutter appears impossible in subsonic and transonic flows, SDOF torsional flutter is possible, at least from an aerodynamic work standpoint. Euler-based calculations indicate that an SDOF torsional flutter instability exists near the bottom of the transonic dip, for moderately high mass ratios. This SDOF instability is very different from the linear subsonic SDOF torsional flutter described in the classical literature (Runyan, 1952), which requires very low reduced frequencies and a torsional axis forward of the quarter chord.

The SDOF torsional flutter can usually only be observed indirectly, through its interaction with the bending–torsion flutter mode, as in Fig. 6. Only the least stable aeroelastic mode is generally observable in a wind tunnel test, or in a time-marching flutter simulation, and in most cases this is the bending–torsion flutter mode. But at sufficiently high mass ratios, the "naked" SDOF instability near the bottom of transonic dip does emerge; see Fig. 7. Shock–boundary layer interactions and 3-D effects no doubt influence this instability, but recent wind tunnel test data (Knipfer and Schewe, 1999) suggest that it can be observed under the right conditions.

3.3. Flutter–divergence interactions

For transonic Mach numbers close to where the peaks of $C_{L\alpha}$ and $C_{M\alpha}$ occur, the typical section wing model tends to diverge. Because the lift and moment coefficient slopes are singular in the limit $\delta \to 0$ (Bendiksen, 2002), divergence seems assured, if the aerodynamic center is ahead of the elastic axis. But the divergence is "weak" in the sense that the new nonlinear equilibrium position is typically at a small elastic twist and is stable.

Although triggered by the "almost singular" lift curve slope, the weak divergence and flutter–divergence interactions do not occur at the Mach number where the lift curve slope peaks, because the aerodynamic center (AC) moves aft with increasing Mach number, which decreases the AC–EA offset e. Thus, the peak value of $eC_{L\alpha}$ will occur at a lower Mach number than the bottom of the transonic dip. For the NACA 0012 model the shift is about 0.05, and weak divergence and flutter–divergence interactions occur around Mach 0.80. Examples of weak divergence and flutter–divergence interactions are shown in Fig. 8.

Whenever weak divergence is possible, the classical flutter boundary is ill-defined, because flutter–divergence interactions occur. In some cases, flutter occurs as a secondary Hopf bifurcation, Fig. 9, and a linear flutter boundary does not exist in the classical sense. At low mass ratios, the flutter mode that emerges is often of a very low frequency, outside the bending–torsion frequency band; see Fig. 10.

4. Flutter via period-tripling bifurcations

4.1. Anomalous μ-scaling

Near the transonic dip, the flutter boundary scaling with respect to μ does not approach the asymptotic $\sqrt{\mu}$ scaling expected from linear subsonic theories for high values of μ. This observation has a number of practical consequences.

The anomalous μ-scaling and the SDOF torsional instability are closely related to the "almost singular" (a.s.) behavior of the lift curve slope, as discussed by Bendiksen (2002). The abnormal scaling could be relevant in wind tunnel tests, where the mass ratio often varies over a significant range in a single model test.

Fig. 11 shows the dependence of the transonic flutter boundary on mass ratio, μ, for the NACA 0012 Benchmark Model at the bottom of the transonic dip ($M_\infty = 0.85$). At high mass ratios a significant drop in the flutter dynamic pressure occurs as the SDOF torsional flutter instability emerges, replacing the bending–torsion instability. At very low mass ratios, a period-tripling bifurcation of the flutter mode is observed, Figs. 12–15. For mass ratios of roughly 400 and above, the "naked" SDOF torsional flutter instability can be observed. As the SDOF torsional flutter emerges, the reduced airspeed at flutter approaches an asymptotic value close to $1/k_\alpha^c$, where k_α^c is the critical (maximum) reduced frequency at which SDOF torsional flutter is possible for this model at this Mach number and angle of attack. Simultaneously, the speed index and the dynamic pressure at flutter continue to drop with increasing μ, as shown in Fig. 11.
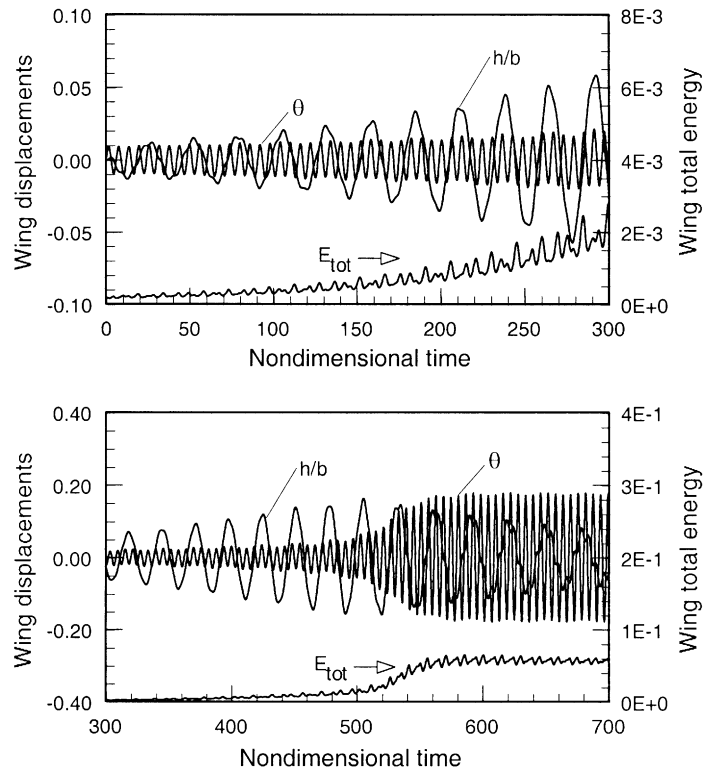
Fig. 6. Emergence of SDOF torsional flutter near the transonic dip, resulting in multibranch flutter where both bending and torsion branches are unstable, but remain far apart in frequency (NACA 0006 model at Mach 0.882; $\mu = 1600$; $\bar{U} = 9.768$).
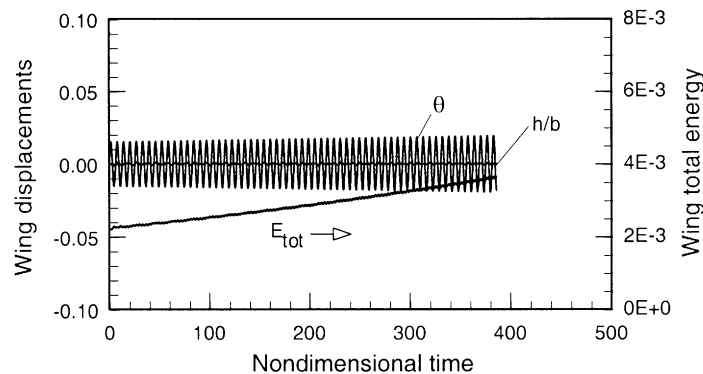

Fig. 7. SDOF torsional flutter near the bottom of the primary transonic dip of the NACA 0012 model ($M_\infty = 0.85$; $\mu = 2000$; $\bar{U} = 4.5$; $g = 0.0024$).

4.2. Period-tripling flutter

As the mass ratio is lowered, the reduced frequency at which flutter occurs increases. Below a mass ratio of roughly 2–5, linear theories predict that flutter should become impossible; i.e., the flutter speed should approach infinity. But in the transonic region, at least, our calculations show that the flutter speed does not approach infinity at very low mass ratios; see Fig. 11. Instead, the aerodynamic nonlinearities open up a new route to flutter, whereby the reduced frequency of the critical aeroelastic mode is lowered into the unstable range through a period-tripling bifurcation. This flutter occurs at a frequency outside the first bending–first torsion frequency interval, and cannot be understood within a linear flutter analysis framework.
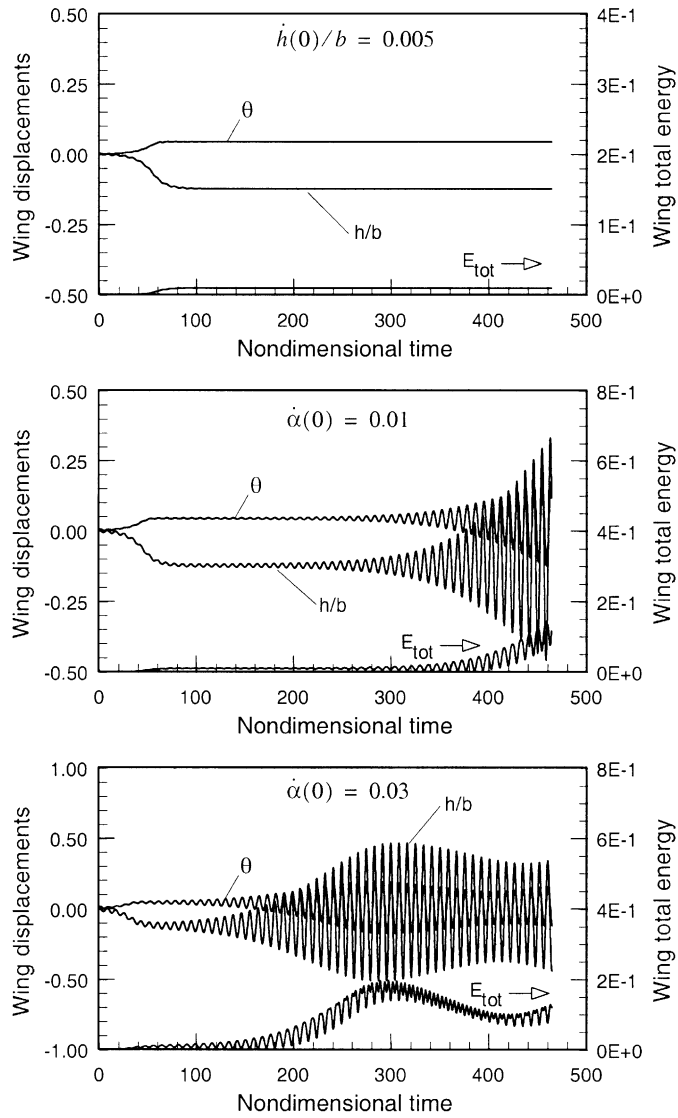
Fig. 8. Examples of weak divergence and flutter–divergence interactions in transonic flow. Note sensitivity to initial conditions (NACA 0012 model; $M_\infty = 0.80$; $\mu = 25$; $\bar{U} = 2.5$; $g = 0.0024$).
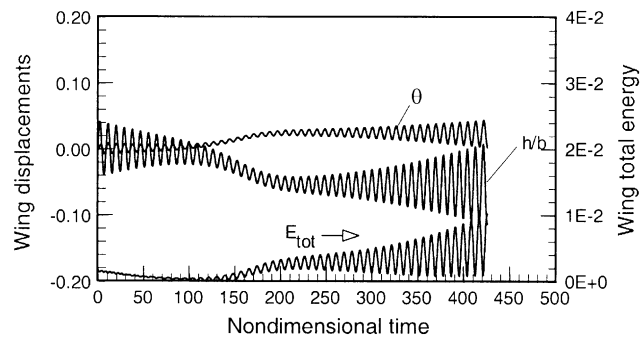

Fig. 9. Weak divergence can trigger flutter via a secondary Hopf bifurcation (NACA 0012 model; $M_\infty = 0.80$; $\mu = 50$; $\bar{U} = 3.05$; $g = 0.0024$).
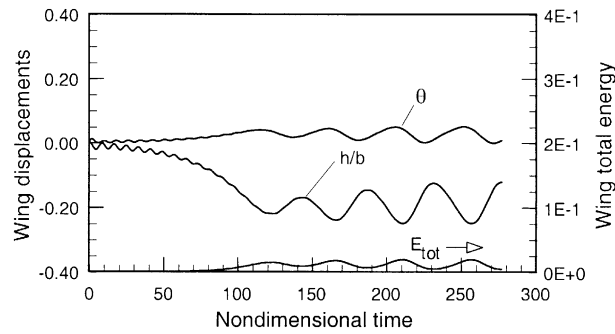
Fig. 10. Flutter–divergence interactions triggering low-frequency flutter at low mass ratio. The flutter frequency is roughly 0.178 of the initial bending-branch frequency before flutter occurs (NACA 0012 model; $M_\infty = 0.82$; $\mu = 5$; $\bar{U} = 1.5918$; $g = 0.0024$).
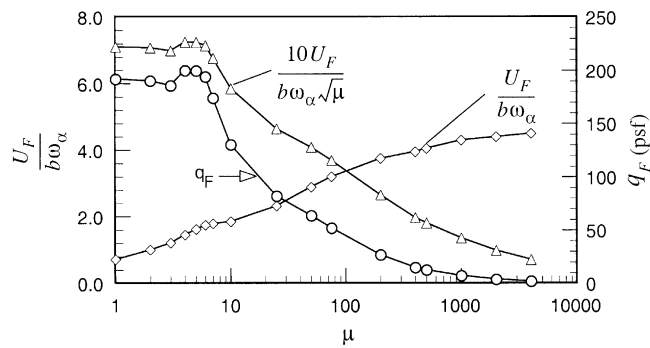

Fig. 11. Flutter boundary vs. mass ratio for the NACA 0012 Benchmark model at $M_\infty = 0.85$.

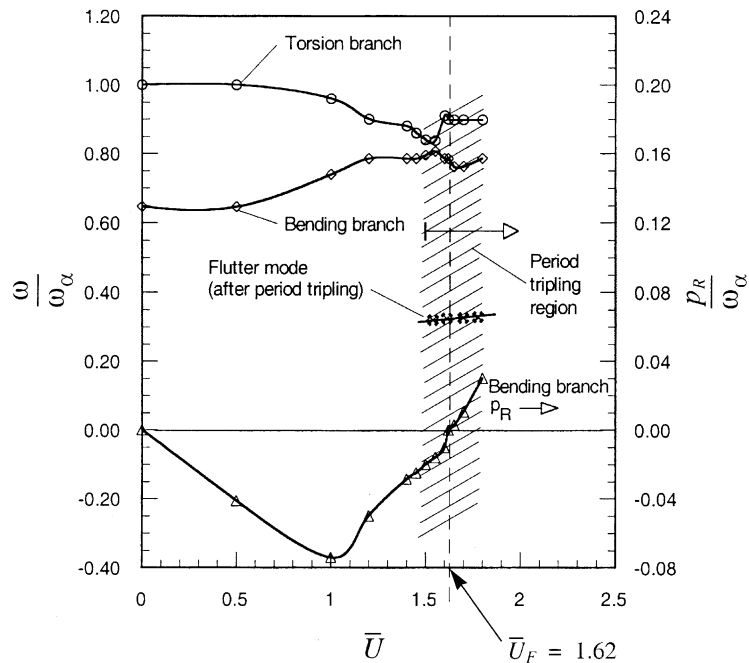Fig. 12. Frequency and damping of aeroelastic modes when period tripling occurs for the NACA 0012 model at Mach 0.85 and $\mu = 5$ ($g = 0.0024$).

Fig. 12 shows the frequency and damping of the bending and torsion aeroelastic branches as a function of reduced airspeed $\bar{U}$, where p_R is the real part of p in the temporal growth e^{pt} of the aeroelastic mode. Fig. 13 shows the emergence of period-tripling flutter, and demonstrates that the period-tripling bifurcation occurs before the flutter boundary is reached (see crosshatched region in Fig. 12). At still lower values for $\bar{U}$, before a coherent $3T$ flutter mode can be observed, the critical aeroelastic mode appears quasiperiodic. Fig. 14 shows that the tripled flutter mode persists to large flutter amplitudes at low mass ratios, but becomes unstable as the mass ratio is increased to $\mu = 6$ and reverts back to a higher-frequency mode with a quasiperiodic appearance. For $\mu \geqslant 7$ no period-tripling flutter was observed, at least not for the NACA 0012 model and the Mach numbers checked, although in some cases the flutter mode appeared quasiperiodic.

Fig. 15 shows the bending–torsion phase plots of the critical aeroelastic mode (bending branch) corresponding to Figs. 12 and 13, before period tripling occurs ($\bar{U} = 1.55$), after period tripling but before flutter ($\bar{U} = 1.60$), and slightly
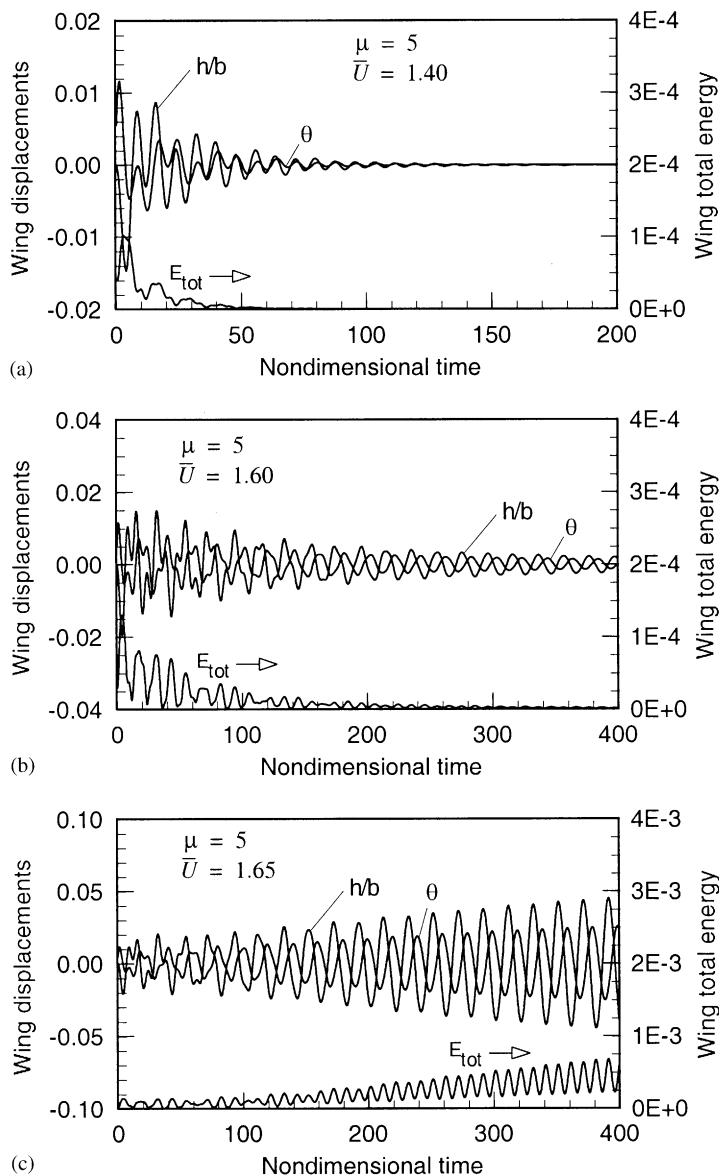

Fig. 13. Period-tripling flutter. Top figure shows stable decay without period tripling. Middle figure shows that the period-tripling bifurcation occurs *before* the flutter boundary is reached. Flutter occurs at a frequency *outside* the $\omega_\alpha - \omega_h$ interval, and can neither be predicted nor understood within a linear flutter analysis framework (NACA 0012 model at $M_\infty = 0.85$; $\dot{\alpha}(0) = 0.03$; $g = 0.0024$).
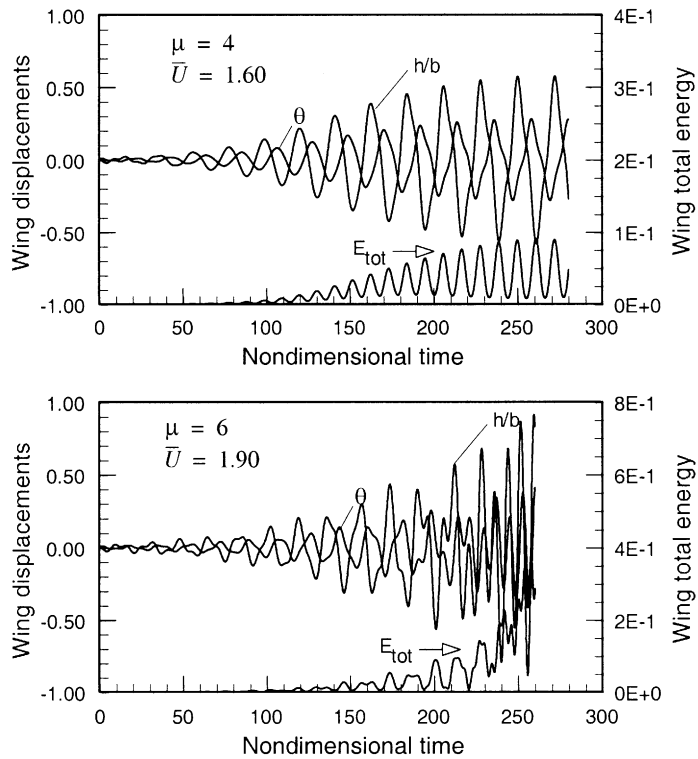
Fig. 14. Illustrating the "stability" of the flutter mode in the post-tripling region at low mass ratios (top figure), even at large flutter amplitudes. At $\mu = 6$ (bottom figure) a modal instability causes a frequency tripling back to the original quasiperiodic (?) flutter mode (NACA 0012 model at Mach 0.85; $g = 0.0024$).
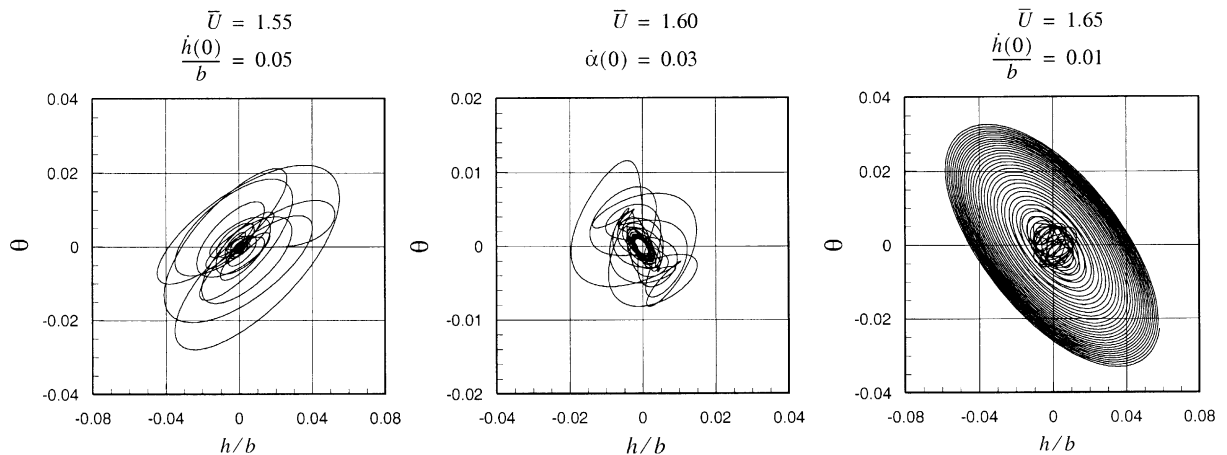

Fig 15. Phase plots of the critical aeroelastic mode immediately before and after period-tripling bifurcation (NACA 0012 model at Mach 0.85; $\mu = 5$; $g = 0.0024$).

beyond the flutter boundary ($\bar{U} = 1.65$). The flutter boundary is at $\bar{U} = 1.62$; see Fig. 12. A close examination of these plots and Figs. 13 and 14 (and numerous others not shown) indicates that the period tripling occurs as follows: (1) adjacent sets of three half-periods are shifted "up" and "down", respectively, in a quasirepetitive temporal pattern; and (2) the middle full period in the $\frac{3}{2}$ sequence is gradually removed by "rectification" (flattening), until the period-tripled mode emerges with a well-defined shape and frequency. The final flutter mode is close to but not exactly one-third of the
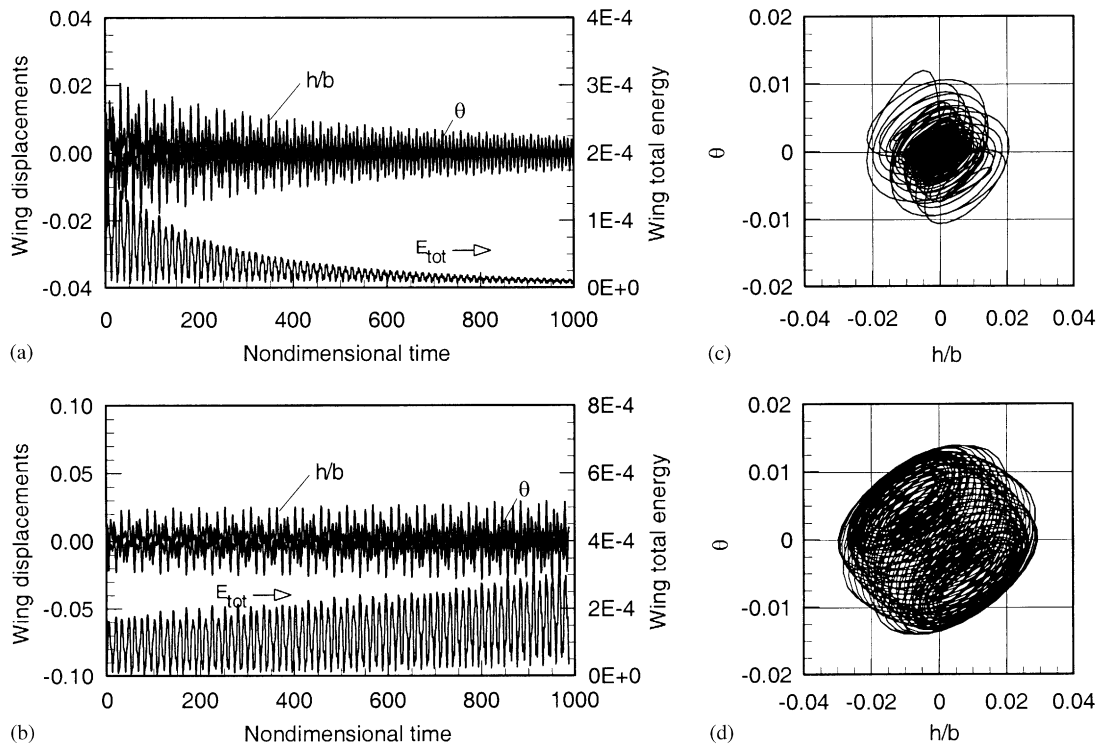
Fig. 16. Almost-periodic (?) or quasiperiodic (?) flutter of NACA 0012 model at Mach 0.85 and $\mu = 6$: (a) at $\bar{U} = 1.75$ (slightly below flutter boundary); (b) at $\bar{U} = 1.77$ (slightly above flutter boundary); and (c and d) corresponding phase plots.

frequency of the parent aeroelastic mode, because of nonlinear effects. In the example shown in Fig. 12, the parent mode is the bending–torsion mode associated with the bending branch.

At the present one can only speculate on why a period tripling and not a period-doubling bifurcation occurs. Both would accomplish the natural task of destabilizing the critical mode sufficiently to cause flutter. But despite a systematic search for period-doubling flutter, none has been found so far. In the period-tripling case, the reduced frequency is decreased from about 0.49 to 0.19, and at the same time the angle by which torsion lags bending increases from close to zero to about $120°$.

In addition to period-tripling flutter, several instances of complex flutter modes were encountered. One such example is shown in Fig. 16. At Mach 0.85 and $\mu = 6$, the NACA 0012 model flutter mode near the linear flutter boundary ($\bar{U} \approx 1.76$) is not a classical mode, nor does period tripling occur. Instead, the mode appears to be either quasiperiodic or possibly almost periodic in the mathematical sense of Bohr (1947). The corresponding phase plots in Fig. 16 reveal a dense set of trajectories that suggests either chaotic or almost-periodic motion.

5. Conclusions

The main conclusions can be summarized as follows:

 (i) Transonic flutter should not be considered "classical" bending–torsion flutter, because flutter near the transonic dip is often triggered by nonlinear interactions between modes. These interactions cannot be understood within the framework of linear coalescence flutter.
 (ii) At high mass ratios, more than one flutter mode (branch) may become active at the same Mach number. This multibranch flutter is not simply a superposition of linear aeroelastic modes, because the superposition principle breaks down and flutter may not necessarily occur when the first aeroelastic eigenvalue crosses into the right half-plane.
(iii) In the transonic region, the flutter speed does not approach infinity at very low mass ratios, as predicted by subsonic linear aerodynamics. Instead, aerodynamic nonlinearities open up a new route to flutter, by lowering the

reduced frequency of the critical aeroelastic mode into the unstable range through a period-tripling bifurcation. This flutter occurs at a frequency outside the first bending–first torsion frequency interval and cannot be predicted by a linear flutter analysis.

(iv) At high mass ratios and Mach numbers near the bottom of the transonic dip, the dynamic pressure drops rapidly as an SDOF torsional flutter emerges. At intermediate mass ratios the SDOF flutter can only be observed indirectly, through its interactions with the bending–torsion mode.

Acknowledgements

References

Anderson, J., 1993. Topological interpretations of non-linear transonic aeroelastic phenomena. Ph.D. Thesis, University of Glasgow, UK.

Anderson, J., 1995. Conjecture on new transonic aeroelastic phenomena. In: Proceedings of the International Forum on Aeroelasticity and Structural Dynamics, 1995, Manchester, England, pp. 84.1–84.11.

Ashley, H., 1980. Role of shocks in the 'sub-transonic' flutter phenomenon. Journal of Aircraft 17, 187–197.

Bendiksen, O.O., 1997a. Fluid–structure coupling requirements for time-accurate aeroelastic simulations. In: Proceedings of the Fourth International Symposium on Fluid–Structure Interactions, Aeroelasticity, Flow-Induced Vibrations and Noise, ASME AD-Vol. 53-3, ASME, New York, pp. 89–104.

Bendiksen, O.O., 1997b. Nonunique solutions in transonic aeroelasticity. In: Proceedings of the International Forum on Aeroelasticity and Structural Dynamics, June 17–20, 1997, Rome, Italy, pp. 425–435.

Bendiksen, O.O., 1991. A new approach to computational aeroelasticity. In: Proceedings of the 32nd AIAA/ASME/ASCE/AHS/ASCE SDM Conference, April 8–10, 1991, Baltimore, MD, USA, pp. 1712–1727.

Bendiksen, O.O., 1999. Improved similarity rules for transonic flutter. AIAA Paper 99-1350, 40th AIAA/ASME/ASCE/AHS/ASCE SDM Conference, April 12–15, 1999, St. Louis, MO, USA.

Bendiksen, O.O., 2001. Energy approach to flutter suppression and aeroelastic control. Journal of Guidance, Control and Dynamics 24, 176–184.

Bendiksen, O.O., 2002. Transonic flutter. AIAA Paper 2002-1488, 43rd AIAA/ASME/ASCE/AHS/ASCE SDM Conference, April 22–25, 2002, Denver, CO, USA.

Bisplinghoff, R.L., Ashley, H., 1962. Principles of Aeroelasticity. Wiley, New York.

Bohr, H., 1947. Almost Periodic Functions. Chelsea Publishing Company, New York.

Garrick, I., 1946. Bending–torsion flutter calculations modified by subsonic compressibility corrections. NACA Report No. 836.

Guckenheimer, J., Holmes, P., 1983. Nonlinear Oscillations, Dynamical Systems, and Bifurcations of Vector Fields. Springer, New York.

Hale, J.K., Verduyn Lunel, S.M., 1993. Introduction to Functional Differential Equations. Springer, New York.

Knipfer, A., Schewe, G., 1999. Investigation of an oscillating supercritical 2D wing section in a transonic flow. AIAA Paper 99-0653.

Lazarus, K.B., et al., 1991. Fundamental mechanism of aeroelastic control with control surface and strain actuation. In: Proceedings of the 32nd AIAA/ASME/ASCE/AHS/ASCE SDM Conference, April 8–10, 1991, Baltimore, MD, USA, pp. 1817–1831.

Rivera, J.A., et al., 1992. NACA 0012 Benchmark model experimental flutter results with unsteady pressure distributions. NASA TM 107581.

Runyan, H.L., 1952. Single-degree-of-freedom flutter calculations for a wing in subsonic potential flow and comparison with an experiment. NACA Report No. 1089.

Theodorsen, T., Garrick, I., 1940. Mechanism of flutter—a theoretical and experimental investigation of the flutter problem. NACA Report No. 685.